



## Synthesis and reactivity of nano-Ag<sub>2</sub>O as an oxidizer for energetic systems yielding antimicrobial products

Kyle T. Sullivan, Chunwei Wu, Nicholas W. Piekielek, Karen Gaskell, Michael R. Zachariah\*

Department of Mechanical Engineering, University of Maryland, College Park, MD 20742, United States  
 Department of Chemistry and Biochemistry, University of Maryland, College Park, MD 20742, United States

### ARTICLE INFO

#### Article history:

Received 13 June 2011  
 Received in revised form 15 November 2011  
 Accepted 17 September 2012  
 Available online 12 December 2012

#### Keywords:

Energetic materials  
 Biocide  
 Pressure cell  
 Time resolved mass spectrometry  
 Nanoaluminum  
 Synthesis

### ABSTRACT

This work investigated Ag<sub>2</sub>O as a potential oxidizer in antimicrobial energetic systems. Ultrafine Ag<sub>2</sub>O was synthesized, and its performance in nanoaluminum-based thermite systems was evaluated using a constant volume combustion cell. The Ag<sub>2</sub>O alone was found to be a relatively poor oxidizer, but it performed well when blended with more reactive oxidizers, CuO and AgIO<sub>3</sub>. Time-resolved mass spectrometry was used to investigate the reaction mechanism in more detail. Post-reaction analysis confirmed the production of Ag, but it was seen to exist in a matrix with Cu in the Al/CuO/Ag<sub>2</sub>O ternary system. The product in surface contact with Al<sub>2</sub>O<sub>3</sub> suggested a reactive sintering mechanism occurred. The results indicate that Ag<sub>2</sub>O, while a poor oxidizer itself, can be integrated into more reactive systems to produce high yields of biocidal silver. The morphology of the final product, however, indicates that a large amount of the silver may not be surface-exposed, a result which would negatively impact the biocidal activity.

© 2012 Published by Elsevier Inc. on behalf of The Combustion Institute.

### 1. Introduction

The effective neutralization of harmful biological agents has become an important topic in the recent literature due to heightened national security concerns of bio-terrorism. Traditional energetic systems, which give rise to short-lived thermal blasts and overpressures, are not ideal for such an application due to risks of inadvertently dispersing the spores. Also, a thermal kill mechanism may not be effective in neutralizing heat-resistant strains of bacteria. These issues have led to increased research on new types of low gas-producing energetic materials which exhibit antimicrobial characteristics long after the exothermic event. A suitable antimicrobial energetic system would produce a high yield of antimicrobial products, in addition to exhibiting good combustion characteristics. The antimicrobial species must function at room temperature, have a large surface area, and be exposed to the environment, i.e. not trapped within a reaction product matrix.

Nanocomposite thermites are currently being investigated as antimicrobial energetic systems. When a metal is mixed with another metal or metal oxide, the resultant thermite reaction gives rise to characteristically high temperatures and low gas production. If the particle size is reduced to the nanoscale, the mixtures are termed nanocomposite thermites [1,2], or Metastable Intermolecular Composites (MICs) [3–5], and exhibit greatly enhanced

reactivity compared to mixtures with micron-sized particles [6,7]. Nanoaluminum (nano-Al) has proven to be an attractive fuel, due to a combination of its low cost and abundance, along with its high reactivity and generation of non-toxic products. Recently, researchers have begun investigating nano-sized oxidizers which produce combustion products exhibiting biocidal capabilities.

One system which has been experimentally studied and shown to display antibacterial activity is AgBr nanoparticle/polymer composites [8]. Other systems include Al/Ag<sub>2</sub>O and Al/I<sub>2</sub>O<sub>5</sub>, and the combustion behavior and biocidal efficacy of these systems have recently been investigated experimentally [9,10]. The authors concluded I<sub>2</sub>O<sub>5</sub> to be a much more effective biocide relative to Ag<sub>2</sub>O due to the large amount of gaseous iodine produced during the reaction. It was found that the silver product remained largely in the condensed phase, thus hindering its effective mass transport to the spores. These two thermite systems were also studied using either mechanical impact or thermal initiation, and measuring flame propagation behavior [11]. The results showed the Al/I<sub>2</sub>O<sub>5</sub> to propagate at 1305 m/s, and the Al/Ag<sub>2</sub>O propagated at 531 m/s, with the energy release rate significantly enhanced by reducing the oxidizer size. We have recently investigated the combustion performance and product morphology of silver iodate (AgIO<sub>3</sub>), a particularly attractive candidate because of its low solubility in water [12]. The ignition temperature was optically measured during rapid Joule heating of a Pt wire, and the combustion behavior was evaluated using a time of flight mass spectrometer [13], along with a constant volume combustion cell. X-ray diffraction confirmed that the major reaction product was AgI, and not elemental

\* Corresponding author at: Department of Mechanical Engineering, University of Maryland, College Park, MD 20742, United States. Fax: +1 301 314 9477.

E-mail address: [mrz@umd.edu](mailto:mrz@umd.edu) (M.R. Zachariah).

silver and iodine. While AgI has been used as an antiseptic [14], at this time there are few studies comparing its efficacy relative to elemental silver and iodine.

A comparison of several silver-based oxidizers is shown in Table 1, along with the theoretically predicted maximum amount of elemental silver produced per gram of mixture. Note that the values of produced silver are given as a theoretical maximum, and will actually be lower if any recombination can occur (as is the case for  $\text{AgIO}_3$ , where the product is largely AgI). From Table 1, it can be seen that  $\text{Ag}_2\text{O}$  can produce the highest amount of elemental silver (86% conversion by mass) relative to the other silver-based oxidizer. Silver has been shown to exhibit antimicrobial characteristics in many forms and at room temperature [15]. As the particle size is reduced and the surface to volume ratio increases, so does the potency of the Ag to bacteria [16]. Also, the presence of an oxide shell has been shown to increase the biocidal activity of silver [17]. The authors claim that silver ions are the actual biocidal species, and a thin oxide shell can promote the release of  $\text{Ag}^+$  to the environment. This sort of behavior may be analogous to what was recently observed for nano-Al with an oxide shell, where molecular dynamics simulation showed that built-in electric fields can serve to facilitate the diffusion of Al ions through the shell [18]. In order to enhance the biocidal activity of an Al/ $\text{Ag}_2\text{O}$  thermite and improve upon its potential as a biocidal energetic system, the mechanism and limitations need further understanding.

In this investigation, ultrafine  $\text{Ag}_2\text{O}$  (<20 nm, measured by TEM) was synthesized by a wet chemical process, and evaluated as an oxidizer in energetic thermite systems, with nano-Al as the fuel. The combustion performance and reaction products of binary Al/ $\text{Ag}_2\text{O}$  mixtures, along with ternary mixtures of Al/ $\text{AgIO}_3$ / $\text{Ag}_2\text{O}$  and Al/ $\text{CuO}$ / $\text{Ag}_2\text{O}$ , were investigated as a function of  $\text{Ag}_2\text{O}$  loading.  $\text{AgIO}_3$  was chosen because it performs very well in combustion tests, and also because its major product, AgI, is likely biocidal in nature.  $\text{CuO}$  was chosen because it is a relatively good oxidizer, but also because of the higher boiling point of Cu (2840 K) relative to Ag (2436 K). This is an important consideration due to the possible formation of core-shell structures governed by the relevant vaporization temperatures. While a variety of oxidizers could potentially enhance the combustion, an oxidizer such as  $\text{Bi}_2\text{O}_3$  may be a poor choice due to the low boiling point (1833 K) of bismuth compared to the boiling point of silver. Upon cooling, a significant amount of Bi may heterogeneously condense onto Ag, rendering an undesirable Ag core/Bi shell morphology. For  $\text{CuO}$ , if heterogeneous condensation occurs, then at least in this case we would expect the silver to condense onto copper, an acceptable morphology with the silver product exposed to the environment. It should be mentioned that elemental copper has been shown to exhibit biocidal capabilities [19–22], and in fact there may be several other metals or alloys which could perform well. The focus at this point has been on using silver and/or iodine, but we want to point out that this is still a largely open question, as there are

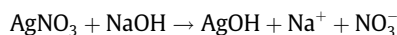
several factors besides room temperature biocidal activity which ultimately will govern this choice.

## 2. Experimental methods

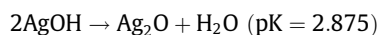
### 2.1. Materials

The nano-Al, termed “50 nm ALEX,” was purchased from the Argonide Corporation. The average particle diameter was 50 nm, as specified by the supplier, and TGA showed the aluminum to be 70% elemental by mass. The copper oxide used in this work was purchased from Sigma Aldrich, and has an average particle diameter of <50 nm as specified by the supplier. The nanoscale  $\text{AgIO}_3$  was synthesized at the Naval Air Warfare Center Weapons Division (NAWCWD) by precipitation from aqueous solutions of silver nitrate and potassium iodate or sodium iodate, using a modification of a literature method [23]. The morphology of the as-produced  $\text{AgIO}_3$  was thin platelets, with the specific surface area measured to be  $4.0 \text{ m}^2/\text{g}$ , corresponding to a spherical particle diameter of 270 nm. More information on the method and characterization can be found in a separate work [12].

The nano-scale  $\text{Ag}_2\text{O}$  was synthesized through a wet chemical technique. A 0.005 M silver nitrate ( $\text{AgNO}_3$ , >99% purity, Sigma Aldrich) aqueous solution was prepared, and 80 mL was heated to 60 °C. 20 mL of a 0.025 M sodium hydroxide ( $\text{NaOH}$ , >98%, anhydrous, Sigma Aldrich) aqueous solution was added drop-wise, while the solution was constantly stirred with a magnetic stir bar, until the solution had the consistency of a gray-yellow colloidal suspension. The reaction of silver nitrate with sodium hydroxide produces silver hydroxide via the following mechanism:



The intermediate AgOH is thermodynamically unstable, and ultimately produces  $\text{Ag}_2\text{O}$  through the following recombination process:



The solution was kept at 60 °C for 2 h to ensure complete reaction. The particles were then collected in 3–4 cycles of a centrifuge/re-dispersion washing process using ethanol, and the solution was allowed to dry, leaving behind the brown  $\text{Ag}_2\text{O}$  particles. A transmission electron microscope image of the as-produced  $\text{Ag}_2\text{O}$  is shown below in Fig. 1. As can be seen, the majority of the primary particles are spherical with diameters <20 nm. The particles have a relatively narrow size distribution, however, are found to be highly

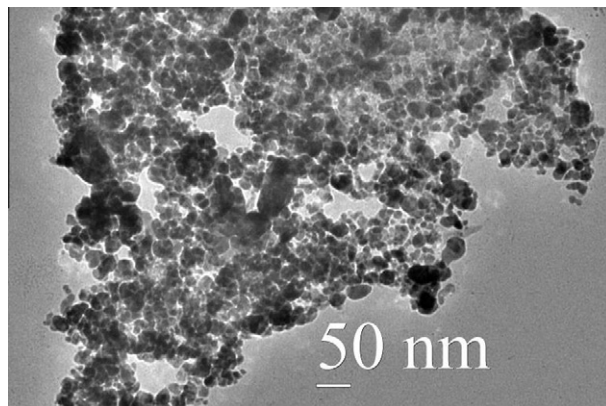


**Fig. 1.** Transmission electron microscope image of the as-produced  $\text{Ag}_2\text{O}$  nanoparticles. The particles are primarily spherical and highly agglomerated. The primary particles are generally <20 nm in diameter.

**Table 1**

Various silver-containing oxidizers and the maximum calculated silver production in stoichiometric thermite mixtures with aluminum. Note that the calculations assume no recombination (i.e.  $\text{Ag} + 0.5\text{I}_2 \rightarrow \text{AgI}$ ) and therefore may overestimate the mass production of silver depending on the extent of recombination.

Oxidizer	Stoichiometric reaction (assuming no recombination)	Grams Ag produced (max)/gram thermite
$\text{Ag}_2\text{O}$	$2\text{Al} + 3\text{Ag}_2\text{O} \rightarrow \text{Al}_2\text{O}_3 + 6\text{Ag}$	0.86
AgO	$2\text{Al} + 3\text{AgO} \rightarrow \text{Al}_2\text{O}_3 + 3\text{Ag}$	0.76
$\text{Ag}_2\text{SO}_4$	$8\text{Al} + 3\text{Ag}_2\text{SO}_4 \rightarrow 4\text{Al}_2\text{O}_3 + 6\text{Ag} + 3\text{S}$	0.56
$\text{AgNO}_3$	$2\text{Al} + \text{AgNO}_3 \rightarrow \text{Al}_2\text{O}_3 + \text{Ag} + 0.5\text{N}_2$	0.48
$\text{AgClO}_4$	$8\text{Al} + 3\text{AgClO}_4 \rightarrow 4\text{Al}_2\text{O}_3 + 3\text{Ag} + 1.5\text{Cl}_2$	0.39
$\text{AgIO}_3$	$2\text{Al} + \text{AgIO}_3 \rightarrow \text{Al}_2\text{O}_3 + \text{Ag} + 0.5\text{I}_2$	0.32

agglomerated into much larger structures. X-ray diffraction (XRD) data for the sample is shown in Fig. 2, and confirms the synthesized material to be  $\text{Ag}_2\text{O}$ .

The thermite samples were prepared by weighing the fuel and oxidizer powders and adding the material to either to a ceramic crucible or glass vial with a few milliliter of hexane. In all samples, the amount of powder was adjusted to only include the active content of aluminum (70 wt%). The dispersions were then ultrasonicated for  $\sim 20$ – $30$  min in a sonicating bath to ensure substantial mixing. For combustion cell tests, the hexane was allowed to evaporate until the samples were completely dry. The dried powder was then very gently broken up using a spatula to remove the larger clumps, and until the consistency was that of a loose powder. To prepare samples for the wire studies, the dispersion was pipetted onto the wire, and the hexane was then allowed to dry before heating was initiated. All mixtures were prepared stoichiometrically assuming complete conversion to  $\text{Al}_2\text{O}_3$ . For the ternary  $\text{Al}/\text{AgIO}_3/\text{Ag}_2\text{O}$  and  $\text{Al}/\text{CuO}/\text{Ag}_2\text{O}$  mixtures, the samples are referred to in terms of the wt% of  $\text{Ag}_2\text{O}$  in the oxidizer.

Any reader should take extreme caution when handling mixed thermites, and especially for sizable masses. Thermite formulations have been found to exhibit high electrostatic sensitivity, and have lower degrees of friction and impact sensitivity as well. Proper grounding equipment and personal protective equipment should be utilized, especially during the synthesis step where the powder is broken up with a spatula. Perhaps the safest rule to handle thermites safely is to prepare the materials in small batches ( $<100$  mg), especially when new formulations are being investigated, as is the case in this work with the ternary mixtures.

## 2.2. Measurement of reactivity

While thermogravimetric analysis and differential scanning calorimetry (TGA/DSC) are the more traditional techniques used to measure and understand reaction kinetics, they employ very slow heating rates (10s of K/min) relative to that predicted in a self-propagating reaction ( $10^4$ – $10^8$  K/s). Therefore, it remains unclear how well this data correlates to such a rapidly heated and likely non-equilibrium combustion. In a recent work [12], we observed that the decomposition behavior of  $\text{AgIO}_3$  was different when the sample was rapidly heated vs. slowly heated in a TGA. While a heating rate dependence may not necessarily translate to other material systems, we have chosen only to use high-heating rate techniques in this work. As prepared, the sample is a loose powder, with an estimated packing density of  $\sim 5\%$  of the theoretical maximum density. While the packing density may change slightly for the different formulations, we do not expect that the density effects will have a significant effect on the reactivity. Thermite mixtures have been shown to transition from a convective to conductive mode of energy transport as the density increases [24],

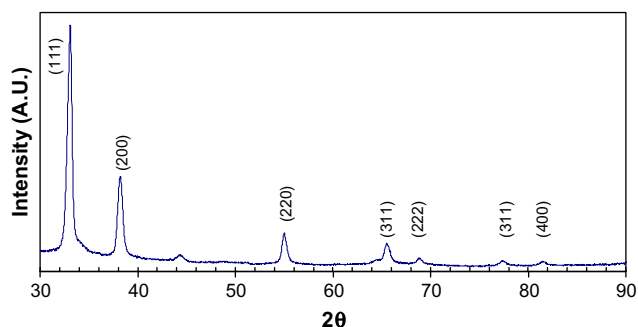


Fig. 2. X-ray diffraction of the as-produced nanoparticles. The labeled peaks confirm the production of  $\text{Ag}_2\text{O}$ .

but this transition is typically at a higher density than what was used in this work. A fixed mass of 25 mg was loaded into a sample holder and combusted inside a constant volume pressure cell ( $\sim 13$  cm<sup>3</sup>). The cell was originally used to only measure the transient pressure signal [4], and was later modified to simultaneously collect the optical emission through a series of lenses coupled to a high-speed photodetector [2]. The transient optical emission and pressure signals are captured during the burning via an oscilloscope, and both can be used to draw conclusions about the combustion behavior. The pressurization rate (peak to peak pressure divided by the pressure rise time) is calculated and is used as a relative measurement of the system reactivity, since it has been shown to scale with flame propagation velocity [5]. The burn time is assigned to be the full width of the optical signal at half maximum. The values of pressurization rate and burn time are specified for our experimental setup, and are only intended to show the relative reactivity. We have found that conclusions about the combustion behavior can be drawn from the relative trends which develop in these measurements as a function of a changing parameter (i.e.  $\text{Ag}_2\text{O}$  mass loading in this work).

Several samples were also investigated using a custom time-of-flight mass spectrometer (TOFMS). In this case, the thermite samples were directly pipetted onto a thin Pt wire. The wire was then supplied a tunable current pulse, and undergoes Ohmic heating at rapid heating rates ( $T_{\text{max}} \sim 2000$  K at  $\sim 5 \times 10^5$  K/s). A series of mass spectra is collected every 100  $\mu\text{s}$  to resolve transient speciation during the decomposition or chemical reaction. The details of this setup can be found elsewhere [13].

## 2.3. Post-reaction analysis

The reacted sample was collected after combustion in the pressure cell, and was analyzed using various techniques. X-ray diffraction (XRD, Bruker C2 Discover with GADDS, operating at 40 kV and 40 mA with unfiltered Cu  $K\alpha$  radiation,  $E = 8049$  eV,  $\lambda = 1.5406$  Å) was used to determine the crystalline species produced during the reaction. Transmission electron microscopy (TEM, JEOL 2100F) coupled with energy dispersive X-ray spectroscopy (EDS, Oxford INCA 250) was used to analyze the product and determine the morphology of the silver in the product. X-ray photoelectron spectroscopy (XPS) data was collected using a Kratos Axis 165 system operating in hybrid mode, with monochromatic aluminum X-rays (1486.5 eV). Survey spectra and high resolution spectra were collected with pass energies of 160 eV and 20 eV, respectively. Samples were mounted on double sided carbon tape. Charge neutralization was required to minimize sample charging, all peaks were calibrated to the adventitious hydrocarbon peak at 284.8 eV.

## 3. Results and discussion

### 3.1. Combustion performance

The pressure cell results for each binary thermite system are shown in Table 2. The  $\text{AgIO}_3$  significantly outperforms both oxidizers, which has been suggested to be largely attributed to iodine gas release during the decomposition of the oxidizer [12]. The  $\text{Al}/\text{Ag}_2\text{O}$  system performed very poorly in pressurization rate when compared to a relatively common and reactive thermite,  $\text{Al}/\text{CuO}$ . A comparison of thermodynamic equilibrium predictions for  $\text{Al}/\text{CuO}$  and  $\text{Al}/\text{Ag}_2\text{O}$  thermites is shown in Table 3. These values are taken from a publication by Fisher and Grubelich [25], and were constant enthalpy and pressure (HP) equilibrium calculations assuming phase changes. Based on our experimental approach, it would be ideal to redo these calculations as constant volume and internal energy calculations, while including the mass of  $\text{Al}_2\text{O}_3$

**Table 2**

Experimental results for the three thermite systems used in this work. All oxidizers were mixed with nano-Al with an equivalence ratio of 1.

	Al/AgIO <sub>3</sub>	Al/CuO	Al/Ag <sub>2</sub> O
Pressure rise (psi)	296 (2041 kPa)	116 (800 kPa)	10.0 (68.9 kPa)
Pressure rise time (μs)	5.3	13	1459
Pressurization rate (psi/μs)	57 (385 kPa/μs)	9.0 (61.5 kPa/μs)	0.002 (0.047 kPa/μs)
FWHM burn time (μs)	172	192	1381

**Table 3**

A comparison of thermodynamic equilibrium predictions of Al/CuO and Al/Ag<sub>2</sub>O thermites. Calculations are from Fischer and Grubelich [25] and assume constant enthalpy and pressure with phase changes taken into account.

Reaction	$\rho_{TMD}$ (g/cm <sup>3</sup> )	$T_{AD}$ (K)	Moles gas per 100 g	Primary gas at equilibrium
2Al + 3CuO → Al <sub>2</sub> O <sub>3</sub> (L) + 3Cu(L,g)	5.109	2843	0.5400	Cu
2Al + 3Ag <sub>2</sub> O → Al <sub>2</sub> O <sub>3</sub> (L) + 6Ag(L,g)	6.386	2436	0.4298	Ag

from the thin oxide shell. However, several of the silver-containing species were not currently present in the thermodynamic database of the CHEETAH or NASA Chemical Equilibrium with Applications (CEA) software, and so an accurate calculation was not possible. As a comparison, a stoichiometric mixture of Al/CuO run with CHEETAH at constant volume and internal energy, and accounting for the 30 wt% oxide shell, changes the adiabatic flame temperature to 2962 K compared to 2836 K. While not insignificant, it can be seen that the difference is relatively small compared to the values reported by Fisher and Grubelich.

Looking at Table 3, we see that both Al/CuO and Al/Ag<sub>2</sub>O are predicted to produce a relatively large amount of equilibrium gas (mostly comprised of the metal, Cu or Ag), and the systems are comparable in terms of the density. However, the Al/Ag<sub>2</sub>O was found to react poorly, while the Al/CuO system reacts violently. This is inconsistent with other work which showed Al/Ag<sub>2</sub>O to react quite vigorously (propagation velocity of 531 m/s) in an instrumented burn tube [11]. This value is very close to the flame propagation velocity of Al/CuO, which has been measured via a similar method [26], and so one would expect the two systems to be comparable in terms of reactivity. However, one major difference between our results and the burn tube results is that our reaction is unconfined, and at a very low packing density. It would appear that these factors alone may be enough to significantly change the combustion performance, with an observed almost four orders of magnitude difference in the combustion behavior between Al/CuO and Al/Ag<sub>2</sub>O.

We have recently argued that the oxidizer decomposition is primarily responsible for pressurizing the system if the oxidizer can be decomposed efficiently, and on a timescale faster than the burn time of the fuel [2]. According to the ICT Database of Thermochemical Values, Ag<sub>2</sub>O has an enthalpy of formation of −31 kJ/mol and a decomposition temperature of 523 K. As a comparison, CuO has an enthalpy of formation of −156 kJ/mol, and calculations using the NASA CEA software predict it to start decomposing near 1100 K at atmospheric pressure. From these thermodynamic considerations, we would expect Ag<sub>2</sub>O to decompose similarly, if not more readily than CuO, as its decomposition is less endothermic and occurs at a lower temperature. The reacted Al/Ag<sub>2</sub>O was collected from the combustion cell and examined with XRD, the results of which are shown in Fig. 3. It can be seen that there is some residual Ag<sub>2</sub>O detected in the product, indicating that the reaction was not even vigorous enough to fully decompose the low-enthalpy Ag<sub>2</sub>O.

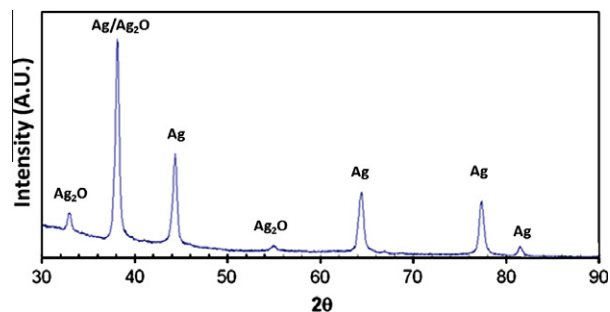


**Fig. 3.** X-ray diffraction of reacted Al/Ag<sub>2</sub>O. Note the presence of Ag<sub>2</sub>O even after the reaction, indicating that some of the oxidizer was not fully decomposed. Note that there is no Al<sub>2</sub>O<sub>3</sub> signal, as the product is amorphous and does not show a strong diffraction peak.

To further examine the relative difference between Ag<sub>2</sub>O and CuO as oxidizers, we turn to the TOFMS results. The O<sub>2</sub> release profile is shown for the binary thermites Al/CuO and Al/Ag<sub>2</sub>O in Fig. 4. What can be seen is that the relative intensity of O<sub>2</sub> release is similar, if not higher, for Al/Ag<sub>2</sub>O than it is for Al/CuO. It can also be seen that the onset of O<sub>2</sub> release occurs earlier (about 400 K lower) in the Al/Ag<sub>2</sub>O system than it does for Al/CuO. These results are consistent with the thermodynamic considerations, where Ag<sub>2</sub>O has a lower enthalpy of formation and decomposition temperature than CuO. If the O<sub>2</sub> release rate can be used as a relative measurement of the reactivity, then this analysis alone would suggest Ag<sub>2</sub>O to be a better oxidizer than CuO. However, the transient behavior of the O<sub>2</sub> release must be considered, specifically in a loose powder unconfined experiment where the O<sub>2</sub> has the potential to escape. For the Al/Ag<sub>2</sub>O sample, it is possible that the reduced temperature of O<sub>2</sub> release leads to some amount of the oxidizing gas escaping the sample before the reaction becomes vigorous for combustion.

Another factor which may explain the difference in reactivity is the different adiabatic flame temperatures. These temperatures are 2843 K and 2436 K for Al/CuO and Al/Ag<sub>2</sub>O, respectively. For Al/Ag<sub>2</sub>O, the adiabatic temperature is much closer to the melting temperature of Al<sub>2</sub>O<sub>3</sub> (2327 K), and the inability to rapidly melt Al<sub>2</sub>O<sub>3</sub> could retard the kinetics of the reaction for several reasons, including:

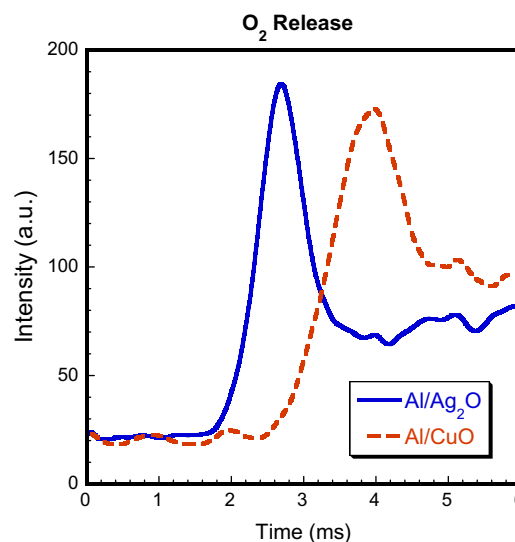


**Fig. 4.** O<sub>2</sub> release profile of Al/Ag<sub>2</sub>O and Al/CuO binary mixtures, as measured using a custom TOF-MS setup. The intensity of the O<sub>2</sub> peak is similar in both systems, but the onset occurs earlier (~400 K lower temperature) in the Al/Ag<sub>2</sub>O thermite.

1. Nanoaluminum is naturally passivated by a few nanometer thick  $\text{Al}_2\text{O}_3$  shell [27,28], and the phase of the shell may greatly affect the outwards mass transport rate of Al. This assumes a diffusion-based reaction mechanism occurs for nano-Al [28,29,18].
2. If the temperature is too low that the oxide product is solid instead of molten, it provides a substantial diffusion barrier between the fuel and oxidizer which increases in thickness as the reaction proceeds.

While we are not certain what is the primary contributing factor to the low reactivity of the Al/Ag<sub>2</sub>O, it seems reasonable to suggest that it is an artifact of some combination of O<sub>2</sub> escape and the difference in adiabatic flame temperatures. It has been shown that the reactivity in thermites is more sensitive to gas production than reaction temperature [26]. However, the result may be different if, for example, the temperature drops below a critical value and effectively changes the rate of mass diffusion.

Next we turn to ternary thermite systems consisting of nano-Al and blends of Ag<sub>2</sub>O with more reactive oxidizers, AgIO<sub>3</sub> and CuO. The pressurization rates of the ternary systems are presented in Fig. 5. All data has been normalized by the pressurization rate of the corresponding binary systems, Al/AgIO<sub>3</sub> and Al/CuO, in order to discuss the relative performance. For the Al/AgIO<sub>3</sub>/Ag<sub>2</sub>O system, the pressurization rate decreased steadily as Ag<sub>2</sub>O was added until 45 wt% Ag<sub>2</sub>O, where there was a very sudden and sharp drop. For the Al/CuO/Ag<sub>2</sub>O system, the pressurization behavior remained relatively unchanged until >70 wt% Ag<sub>2</sub>O. Above this value a steady decrease was observed until >95 wt% Ag<sub>2</sub>O, where it finally dropped to a low value. Even at 87 wt% Ag<sub>2</sub>O, the pressurization rate had only decreased by a factor of two, indicating that a large amount of Ag<sub>2</sub>O can be incorporated into the Al/CuO thermite with little decrease in the reactivity.

Next we look at the measured burning times, which are shown for the two ternary systems as a function of mass loading of Ag<sub>2</sub>O

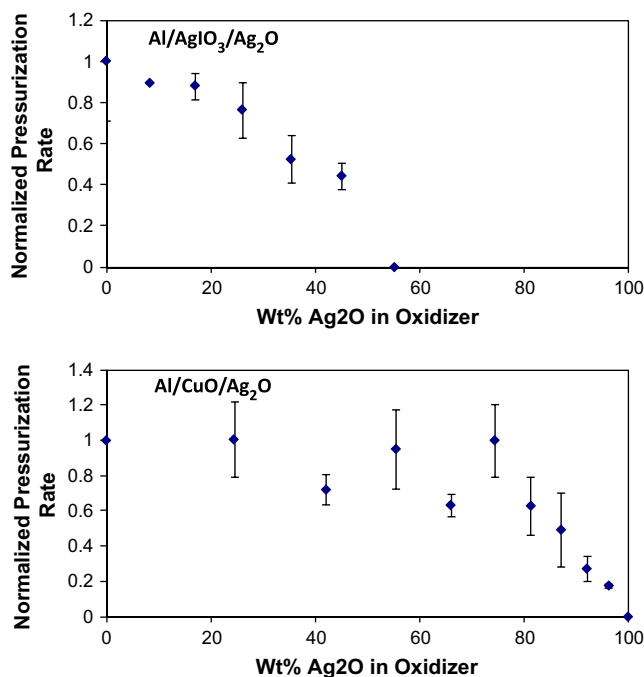


Fig. 5. Experimental results for the Al/AgIO<sub>3</sub>/Ag<sub>2</sub>O (top) and Al/CuO/Ag<sub>2</sub>O systems (bottom). Values have been normalized by pure Al/AgIO<sub>3</sub> and pure Al/CuO for the top and bottom, respectively. All mixtures are stoichiometric with an equivalence ratio of 1 assuming complete reaction to Al<sub>2</sub>O<sub>3</sub>.

in Fig. 6. What can be seen is that the burn time stays relatively constant as Ag<sub>2</sub>O is added to both systems. Above 45% in the Al/AgIO<sub>3</sub>/Ag<sub>2</sub>O system there is a sudden and sharp increase in the burning time, and this is also the point where the pressurization rate was found to decrease suddenly. For the Al/CuO/Ag<sub>2</sub>O thermite the burn time remains relatively constant over the entire range of added Ag<sub>2</sub>O, and does not increase suddenly until the oxidizer is 100% Ag<sub>2</sub>O.

The pressurization rate and burn time measurements show that Ag<sub>2</sub>O can display good reactivity, but only when blended with other oxidizers. As mentioned before, several of the species which may be of interest (i.e. AgI and AgO) are currently not contained within the thermodynamic product library of the NASA CEA or CHEETAH software, and therefore equilibrium calculations are not included. However, adding both AgIO<sub>3</sub> and CuO will serve to increase the adiabatic flame temperature over that of Al/Ag<sub>2</sub>O, and apparently even a slight increase in temperature can significantly enhance the performance of Ag<sub>2</sub>O. This is especially clear in the Al/Ag<sub>2</sub>O/CuO system, where the reactivity is increased orders of magnitude relative to Al/Ag<sub>2</sub>O when a mere 5 wt% of CuO (95% Ag<sub>2</sub>O) is added. As was previously discussed, other works have shown Al/Ag<sub>2</sub>O and Al/CuO to exhibit comparable flame velocities in burn tubes [11,26]. In this work, we observe that in unconfined burn tests of loose powders, Al/Ag<sub>2</sub>O on its own reacted poorly, but with a small addition of CuO the system became quite reactive and approached the reactivity of Al/CuO.

### 3.2. Post-reaction analysis

The reacted product was collected for each sample and studied using XRD to determine the crystalline product species. The diffraction patterns for the Al/AgIO<sub>3</sub>/Ag<sub>2</sub>O system are shown in Fig. 7. As can be seen, the strongest peak of Ag at  $2\theta = 38.15^\circ$  from the (1 1 1) plane increases with the mass loading of Ag<sub>2</sub>O, while the strongest peak of AgI at  $2\theta = 23.81^\circ$  from (1 1 1) plane decreases. Above 40% the relative intensity of both peaks decreases, corresponding to the point where the pressurization rate was observed

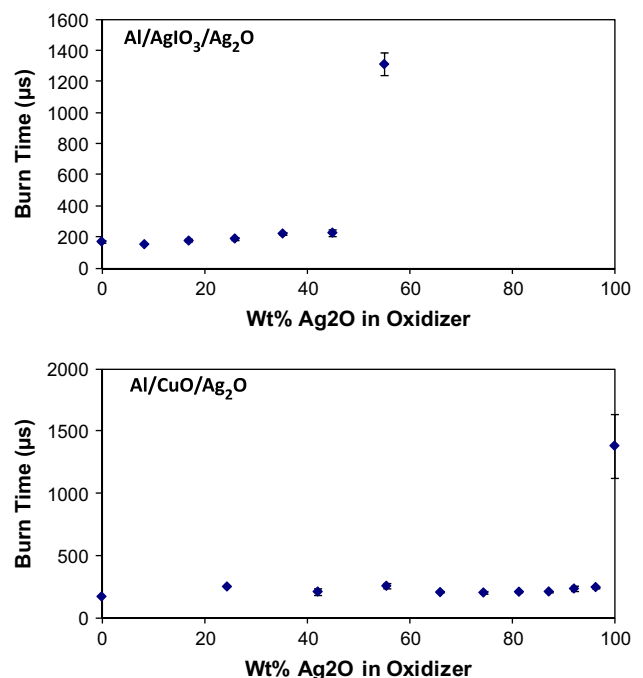


Fig. 6. Burn time (full width half max of optical signal) as a function of Ag<sub>2</sub>O mass loading for Al/AgIO<sub>3</sub>/Ag<sub>2</sub>O (top) and Al/CuO/Ag<sub>2</sub>O (bottom).

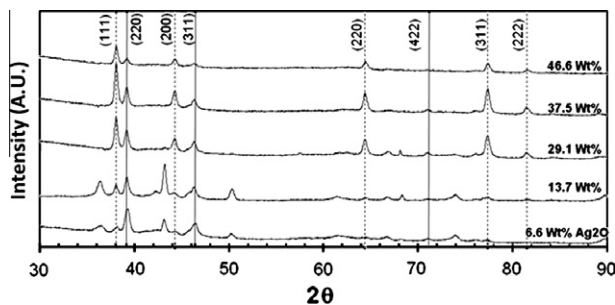


Fig. 7. X-ray diffraction of the reacted Al/Ag<sub>2</sub>O/Ag<sub>2</sub>O samples collected after combustion in the pressure cell. The dotted vertical lines are Ag peaks, while the bold lines are AgI. XRD confirms the formation of elemental silver, along with decreasing amounts of AgI as the Ag<sub>2</sub>O mass loading increases. Above 45 wt%, a drop in the intensity of both Ag and AgI is observed, indicating a shift in the reaction mechanism, and experimentally supported by a sudden drop in the pressurization rate and increase in burn time.

to rapidly decrease. The XRD data for the Al/CuO/Ag<sub>2</sub>O system is shown in Fig. 8. The Ag peaks are all present, however, only trace amounts of crystalline Cu were detected in the product relative to the amount of Ag. It is possible that some of the reduced copper can re-oxidize with the air in the pressure cell to form an amorphous product, or the Cu quenches so rapidly that it cannot re-crystallize within this timescale. Another possibility is that some amount of the Ag and Cu can alloy, however we would expect the intensity of the silver peaks would reflect this trend if this were happening. From Fig. 8, no obvious trend in the intensity of the Ag peaks was observed with increased mass loading of Ag<sub>2</sub>O. This may partially be caused by differing sample sizes used in the XRD; however, it is a curious observation which we do not have a strong explanation for at the given time. XPS was performed on selected samples from each ternary system, and confirmed the production of surface-exposed Ag. Details of the analysis are included as an Appendix A.

A small amount of the reacted product was collected and investigated with a TEM. The Al/Ag<sub>2</sub>O/AgIO<sub>3</sub> is not included, since EDS could not easily distinguish between elemental Ag and AgI. Also, significant morphological changes were induced by the electron beam, thus making imaging and elemental analysis nearly impossible. Since AgI is considered a biocidal species itself, identifying its relative position to Ag is of less importance than looking at a non-biocidal species, such as Cu relative to Ag. Therefore, only results for Al/Ag<sub>2</sub>O/CuO are shown. The sample chosen to investigate was 74 wt% Ag<sub>2</sub>O, which corresponds to the maximum amount of Ag<sub>2</sub>O which resulted in no loss to the reactivity (see Fig. 5). A TEM image, along with corresponding elemental maps is shown in Fig. 9.

What can be seen is that the produced Ag/Cu is in surface contact with a product containing Al and O. The Ag and Cu positions are found to almost entirely overlap. Again, it is possible that some

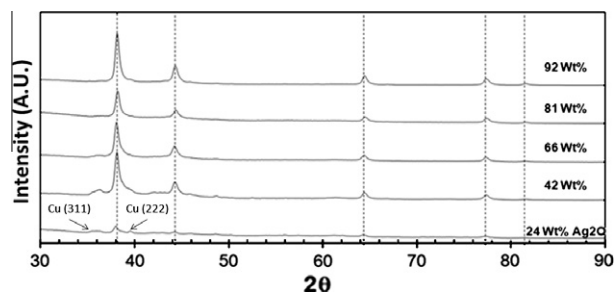


Fig. 8. X-ray diffraction of the reacted Al/CuO/Ag<sub>2</sub>O samples collected after combustion in the pressure cell. The dotted vertical lines represent the Ag peaks.

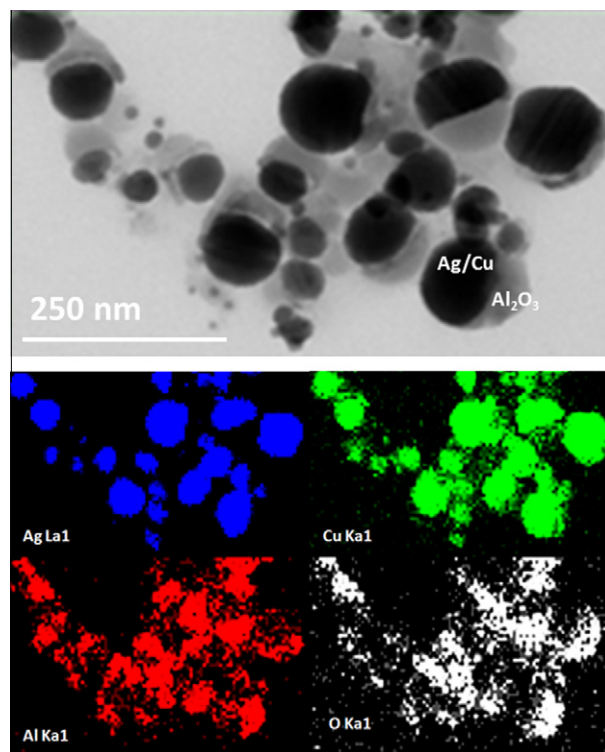
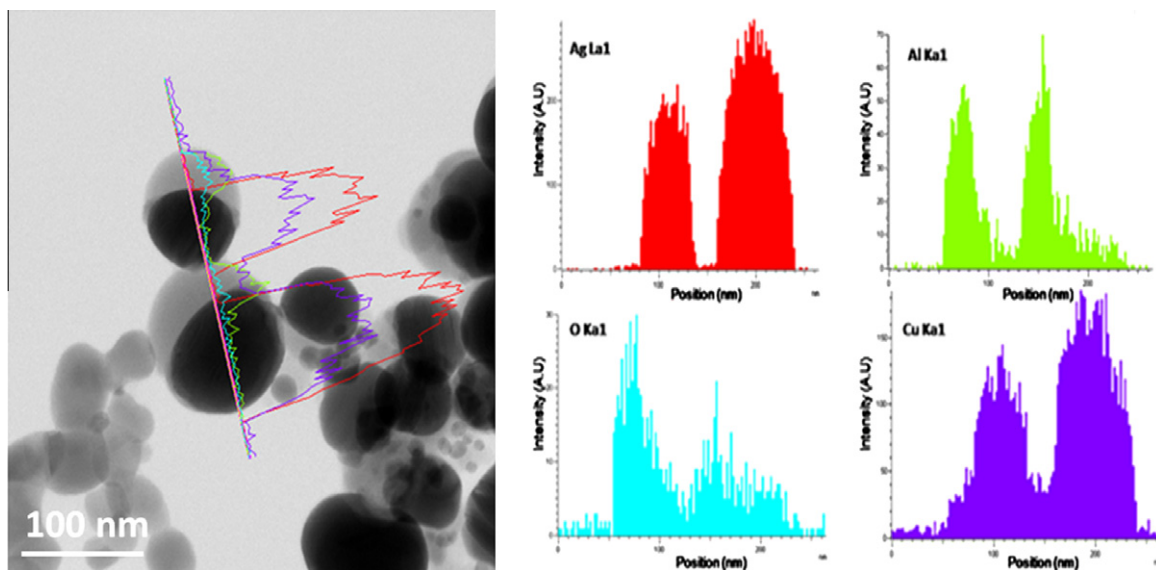


Fig. 9. Image and elemental mapping (white boxed region) of Al/74 wt% Ag<sub>2</sub>O/26 wt% CuO, corresponding to the maximum Ag<sub>2</sub>O added before a significant decrease in the reactivity was seen. The results show Al<sub>x</sub>O<sub>y</sub> is in surface contact with a product which is a combination of both Ag and Cu.

Ag/Cu alloy can form, but this has not been quantified if it is occurring. What can also be seen is that the large aggregated Ag<sub>2</sub>O nanoparticles (<20 nm diameter, see Fig. 1) have sintered into characteristically larger and more spherical structures, in surface contact with the oxide product. The resultant morphologies are not consistent with a mechanism in which the Ag product had vaporized and recondensed. To further characterize the observed morphologies, an elemental linescan was performed and is shown in Fig. 10. The linescan shows that the lighter material corresponds to Al and O, whereas the dark material is a mix of both Ag and Cu. The results are consistent with a reactive sintering mechanism, which has recently been observed for several nano-Al based thermites [30,31]. In a reactive sintering mechanism, the reaction occurs at the interface between fuel and oxidizer. As energy is liberated from the exothermic reaction, material is further melted and rapidly delivered to the interface where it continues to react. During this rapid mass transport, some fraction of intermediate gases (i.e. I<sub>2</sub>, O<sub>2</sub>, etc.) may form to drive the pressurization, and a portion of the unburned fuel continues to combust in the oxidizing gaseous environment.

Although the TEM results are interesting from a mechanistic point of view, the implications are negative for biocidal applications. If the fuel and oxidizer create a product which is in surface contact, then a large amount of the produced Ag will not be exposed to the environment post-reaction. While CuO ternary systems can help to increase the reactivity of Ag<sub>2</sub>O up to very high mass loadings of Ag<sub>2</sub>O, the Ag/Cu matrix which forms also will greatly reduce the exposed surface area. If a reactive sintering mechanism, or any other large amount of sintering is indeed occurring, the elemental silver will not maintain the high surface to volume ratio characteristic of the initial Ag<sub>2</sub>O, and will form much larger structures. While all of these points will lead to reduced overall surface area of the produced Ag, the real question for ternary systems will be whether the enhanced reactivity and



**Fig. 10.** Image and elemental linescan across two particles showing the morphology characteristic in the product. The linescan indicates that an Ag/Cu matrix is in surface contact with Al and O (assumed to be  $\text{Al}_2\text{O}_3$ ). Note: The sample is the same as is shown in Fig. 9.

high-yield of elemental Ag outweighs the negative effects, and only further experimental testing can resolve this.

#### 4. Conclusion

Ultrafine  $\text{Ag}_2\text{O}$  powder was synthesized by a wet chemical technique and mixed with nano-Al to form energetic thermite systems designed to produce high yields of antimicrobial silver as a combustion product. The loose powders were combusted in a constant volume pressure cell, where both the transient pressure and optical emission are monitored to investigate performance.  $\text{Ag}_2\text{O}$  itself was found to perform poorly in terms of pressurization rate and burn time, but performed well when combined with two more reactive oxidizers,  $\text{AgIO}_3$  and CuO. In situ time of flight mass spectrometry was used to investigate mechanistic differences between Al/ $\text{Ag}_2\text{O}$  and Al/CuO, and the two were found to behave similarly in that they both released a large amount of  $\text{O}_2$  gas at a comparable rate. It is suggested that the poor reactivity of Al/ $\text{Ag}_2\text{O}$  occurs from some combination of  $\text{O}_2$  gas escape and the low reaction temperature, which is close to the melting point of  $\text{Al}_2\text{O}_3$ . A small amount of CuO, however, can raise the temperature enough for  $\text{Ag}_2\text{O}$  to react violently, as was seen in the ternary system. The relative pressurization rates for both ternary systems were measured. For the Al/ $\text{AgIO}_3$ / $\text{Ag}_2\text{O}$  system, the reactivity dropped off fairly linearly as the mass loading of  $\text{Ag}_2\text{O}$  increased, followed by a sharp drop above 45 wt%. The pressurization rate remained virtually unchanged as the  $\text{Ag}_2\text{O}$  loading was increased in an Al/CuO/ $\text{Ag}_2\text{O}$  system, and had only dropped by about a factor of two when the loading was 87 wt%. This suggested that  $\text{Ag}_2\text{O}$  can behave mechanistically similarly to CuO, and thus the yield of elemental silver produced during the reaction can be dramatically increased with little loss in combustion performance. Ex situ X-ray diffraction (XRD), X-ray photoelectron spectroscopy (XPS), and transmission electron microscopy (TEM) were performed to characterize selected formulations. XRD confirmed the production of crystalline silver, and XPS also detected elemental silver, indicating some amount of the silver was surface-exposed. TEM, however, showed large amounts of the silver product was in surface contact with  $\text{Al}_2\text{O}_3$ , and also was trapped within a matrix of Cu for the Al/CuO/ $\text{Ag}_2\text{O}$  ternary system. It is speculated that a reactive sintering mechanism occurs, and large amounts of the product are sintered

into characteristically larger particles. High-yields of elemental silver can thus be produced in highly reactive ternary formulations, however, the TEM results suggest several factors which could potentially decrease the biocidal efficacy, due to the formation of undesired morphologies which ultimately prevent the silver from being exposed to the environment.

#### Acknowledgments

This work was supported by the Defense Threat Reduction Agency and Army Research Office. We acknowledge the support of the University of Maryland's Nanocenter and its NISPLAB. The NISP laboratory is operated jointly by the Maryland Nanocenter and the NSF MRSEC as a shared experimental facility. We would like to thank Curtis Johnson of the Naval Air Weapons Station China Lake for providing the  $\text{AgIO}_3$ .

#### Appendix A

The following section includes analysis of the materials using X-ray photoelectron spectroscopy. This material is available free of charge via the Internet at <http://pubs.acs.org>.

##### A.1. XPS measurements and analysis

XPS data for silver Ag 3d and Ag MNN were collected for both ternary systems. Data was collected for various wt% of  $\text{Ag}_2\text{O}$  in each system; however, only one set of results will be presented from each system. The data selected is for mixtures with a large wt% of added  $\text{Ag}_2\text{O}$ , but before a significant drop in reactivity was measured. This corresponded to 35 wt%  $\text{Ag}_2\text{O}$  for the Al/ $\text{Ag}_2\text{O}$ / $\text{AgIO}_3$  system, and 87 wt% for the Al/ $\text{Ag}_2\text{O}$ /CuO thermite. A comparison of the spectra before (a and b) and after (c and d) combustion for 35 wt%  $\text{Ag}_2\text{O}$  in Al/ $\text{Ag}_2\text{O}$ / $\text{AgIO}_3$  and 87 wt%  $\text{Ag}_2\text{O}$  in Al/ $\text{Ag}_2\text{O}$ /CuO are shown in Figs. A1 and A2, respectively. Due to very small shifts in binding energy in the Ag 3d region, less than 0.4 eV between Ag,  $\text{Ag}_2\text{O}$  and AgO, it is not possible to discern oxidation state changes based on BE shifts alone. However, the Auger transition exhibits considerable shifts, this two electron hole final state being more sensitive to surrounding environment. Even more convenient is to compare Auger parameters which have the

added benefit of being independent of sample charging and work function. The modified Auger parameter,  $\alpha'$  can be obtained through XPS measurements and is defined as:

$$\alpha' = KE(\text{Auger}) - KE(\text{photoelectron}) + hv$$

where  $KE(\text{Auger})$  is the kinetic energy of an Auger transition,  $KE(\text{photoelectron})$  is the kinetic energy of a core level photoelectron, and  $h\nu$  is the photoexcitation energy.

While the BE shift alone is subtle, the Ag 3d and Auger spectra after combustion are significantly different from that of the starting material for both samples. The Ag 3d peaks show a significant narrowing of the FWHM, the appearance of a second peak and low intensity plasmon loss peaks associated with the Ag 3d 5/2 and 3/2 spin-orbit-split components. The presence of the plasmon peaks which are separated from the most intense Ag 3d 5/2 and 3/2 by  $\sim 3.5$  eV to higher binding energy [32] (labeled with an arrows in the figure) and the narrowed FWHM are characteristic of metal

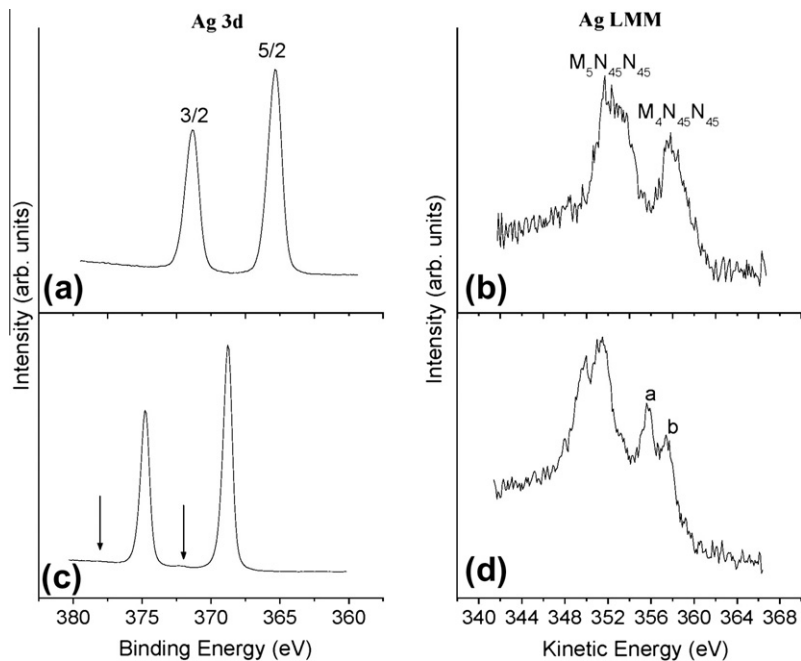


**Fig. A1.** Ag 3d core level and Ag MNN Auger spectra for the  $\text{AgI O}_3$  starting material (a and b) as compared to the spectra from the product of combustion (c and d) for an Al/ $\text{Ag}_2\text{O}/\text{AgI O}_3$  mixture with 35 wt%  $\text{Ag}_2\text{O}$ .

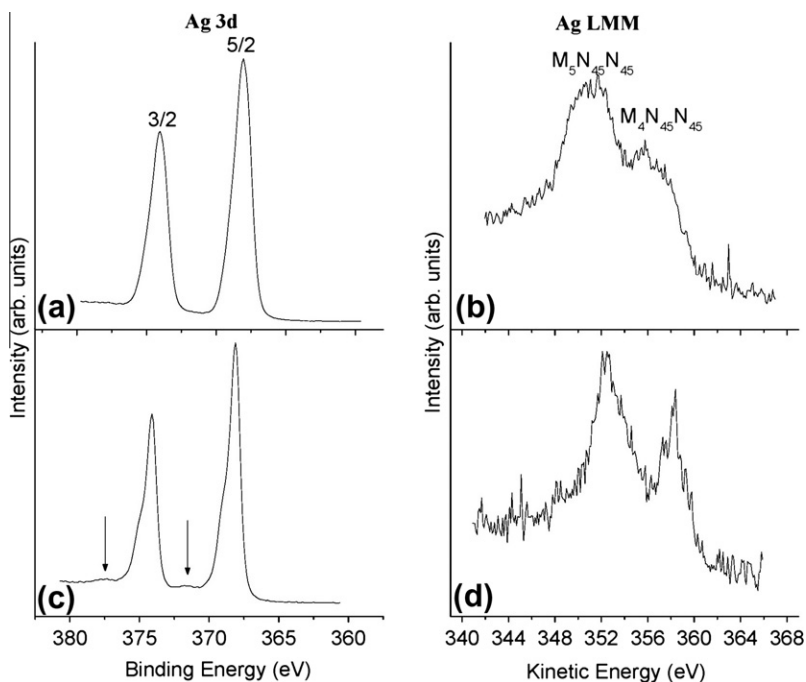


**Fig. A2.** Ag 3d core level and Ag MNN Auger spectra for the  $\text{Ag}_2\text{O}$  starting material (a and b) as compared to the product of combustion (c and d) for an Al/ $\text{Ag}_2\text{O}/\text{CuO}$  mixture with 87 wt% CuO.

**Table A1**  
Modified Auger parameters ( $\alpha'$ ).

	Ag 3d binding energy (eV)	Ag M <sub>4</sub> N <sub>5</sub> N <sub>5</sub> kinetic energy (eV)	$\alpha'$ (eV)
Ag	368.1–368.3 <sup>A</sup>	357.9–358.3	726.0–726.6
AgI	368.0 <sup>A</sup>	356.1 <sup>A</sup>	724.1 <sup>A</sup>
Ag <sub>2</sub> O	368.1 <sup>A</sup> , 368.0 <sup>B</sup>	356.6 <sup>A</sup> , 356.6 <sup>B</sup>	724.4 <sup>A</sup> , 724.3 <sup>B</sup>
AgI <sub>3</sub>	367.9 <sup>B</sup>	355.8	723.7
40% Ag <sub>2</sub> O (AgI <sub>3</sub> )	368.8 <sup>B</sup>	357.4 <sup>B,a</sup> , 355.7 <sup>B,b</sup>	726.2 <sup>B,a</sup> , 724.5 <sup>B,b</sup>
70% Ag <sub>2</sub> O (CuO)	368.1 <sup>B</sup> , 368.9 <sup>B</sup>	358.2 <sup>B</sup>	726.3 <sup>B</sup> , 727.1 <sup>B</sup>

<sup>A</sup> Taken From Ref. [22].

<sup>B</sup> This work.

<sup>a</sup> For AgI.

<sup>b</sup> For Ag.

formation. The appearance of the additional peak at 368.9 eV could be due to the formation of some silver aluminum alloy, as it is in good agreement with literature values, 368.8–369.0 eV [33]. Another possibility is small metallic clusters of silver dispersed on the alumina have also been reported to lead to increases in the Ag 3d binding energy compared to bulk Ag [34]. The Auger parameter of 726.3 eV calculated using the most intense Ag 3d 5/2 peak and the Ag M<sub>4</sub>N<sub>45</sub>N<sub>45</sub> transition is also consistent with the formation of metallic silver.

In Fig. 11, the Ag spectra from the combusted sample differ significantly from both the AgI<sub>3</sub> and Ag<sub>2</sub>O starting materials. The Ag 3d 5/2 for the reacted sample has a FWHM of 0.79 eV and Plasmon loss peaks again both these features are consistent with metal formation. For the MNN Auger peaks shown in Fig. 11d both M<sub>4</sub>N<sub>45</sub>N<sub>45</sub> transition (~356 eV) and M<sub>5</sub>N<sub>45</sub>N<sub>45</sub> transition (~349 eV) seem to be split into two, Auger parameters were calculated using both peaks for the M<sub>4</sub>N<sub>45</sub>N<sub>45</sub> transition, labeled a and b in Fig. 11 and energies reported in Table A1. The binding energy position for the 5/2 peak of 368.8 eV is surprisingly high for pure metallic silver or silver iodide as expected and seen in the X-ray diffraction. Based on the Auger parameter values and XRD results we believe this binding energy to be erroneously high due to differential charging between the hydrocarbon used as the calibration point and the silver. We assign the Auger parameter calculated using peak b ( $\alpha' = 726.2$  eV) to be due to metallic silver and peak

a ( $\alpha' = 724.5$  eV) to be due to silver iodide, their values compared to literature values in Table A1.

## References

- [1] J.J. Granier, M.L. Pantoya, *Combust. Flame* 138 (4) (2004) 373–383.
- [2] K. Sullivan, M.R. Zachariah, *J. Propul. Power* 26 (3) (2010) 467–472.
- [3] W.L. Perry et al., *Propellants, Explos., Pyrotech.* 29 (2) (2004) 99–105.
- [4] A. Prakash, A.V. McCormick, M.R. Zachariah, *Adv. Mater. (Weinheim, Germany)* 17 (7) (2005) 900–903.
- [5] S.F. Son, et al., Propagation studies of metastable intermolecular composites (MIC), in: *Proceedings of the International Pyrotechnics Seminar 2002*, 29th, pp. 203–212.
- [6] C.E. Aumann, G.L. Skofronick, J.A. Martin, *J. Vac. Sci. Technol., B: Microelectron. Nanometer Struct.* 13 (3) (1995) 1178–1183.
- [7] K.B. Plantier, M.L. Pantoya, A.E. Gash, *Combust. Flame* 140 (4) (2005) 299–309.
- [8] V. Sambhy et al., *J. Am. Chem. Soc.* 128 (2006) 9798–9808.
- [9] B.R. Clark, M.L. Pantoya, *Phys. Chem. Chem. Phys.* 12 (39) (2010) 12653–12657.
- [10] C. Farley, M. Pantoya, *J. Therm. Anal. Calorim.* 102 (2) (2010) 609–613.
- [11] R.R. Russell, R.S. Bless, M. Pantoya, *J. Energy Mater.* 29 (2) (2011) 175–192.
- [12] K.T. Sullivan et al., *Combust. Sci. Technol.* 183 (3) (2011) 285–302.
- [13] L. Zhou et al., *Rapid Commun. Mass Spectrom.* 23 (1) (2009) 194–202.
- [14] Merck, in: M.J. O'Neil, et al. (Eds.), *The Merck Index*, 13 ed. Merck & Co., Inc., Whitehouse Station, NJ, 2001.
- [15] E.J. Rentz, *J. Nutr. Environ. Med.* (Abingdon) 13 (2) (2003) 109–118.
- [16] J.R. Morones et al., *Nanotechnology* 16 (10) (2005) 2346–2353.
- [17] A.B. Smetana et al., *Langmuir* 24 (14) (2008) 7457–7464.
- [18] B.J. Henz, T. Hawa, M.R. Zachariah, *Journal of Applied Physics* 107(2) (2010).
- [19] H. Palza et al., *Macromol. Rapid Commun.* 31 (6) (2010) 563–567.
- [20] D. Hamilton et al., *J. Hosp. Infect.* 74 (1) (2010) 62–71.
- [21] G. Moore et al., *Lett. Appl. Microbiol.* 46 (6) (2008) 655–660.
- [22] J. Holton, F. Perna, D. Vaira, *Helicobacter* 11 (4) (2006) 322.
- [23] J. Sendroy, *J. Biol. Chem.* 120 (1937) 335–403.
- [24] C.D. Park et al., *J. Phys. Chem. C* 114 (6) (2010) 2814–2820.
- [25] S.H. Fischer, M.C. Grubelich, Theoretical energy release of thermites, intermetallics, and combustible metals, in: *24th International Pyrotechnics Seminar*, The International Pyrotechnics Society, Monterey, California, USA, 1998.
- [26] V.E. Sanders et al., *J. Propul. Power* 23 (4) (2007) 707–714.
- [27] L.P.H. Jeurgens et al., *Phys. Rev. B: Condens. Matter Mater. Phys.* 62 (7) (2000) 4707–4719.
- [28] M.A. Trunov, M. Schoenitz, E.L. Dreizin, *Combust. Theor. Model.* 10 (4) (2006) 603–623.
- [29] A. Rai et al., *Combust. Theor. Model.* 10 (5) (2006) 843–859.
- [30] K.T. Sullivan, et al., *Applied Physics Letters* 97(13) (2010).
- [31] K.T. Sullivan et al., *Combust. Flame* 159 (1) (2012) 2–15.
- [32] Y. Tachibana et al., *Thin Solid Films* 442 (1–2) (2003) 212–216.
- [33] J.F. Moulder, et al., in: J. Chastain (Ed.), *Handbook of X-ray Photoelectron Spectroscopy*, fifth ed. Perkin-Elmer Co., Eden Prairie, 1992.
- [34] J.A. Rodriguez, M. Kuhn, J. Hrbek, *J. Phys. Chem.* 100 (46) (1996) 18240–18248.